ACS OMEGA

http://pubs.acs.org/journal/acsodf

Article

Controllable Synthesis and Biological Application of Schiff Bases from D-Glucosamine and Terephthalaldehyde

Qinghua Weng, Jinquan Yi, Xiaoping Chen, Dengwang Luo, Yaduan Wang, Weiming Sun, Jie Kang,* and Zhizhong Han*

Cite This: *ACS Omega* 2020, 5, 24864−24870

Read Online

ACCESS | Metrics & More | Article Recommendations | Supporting Information

ABSTRACT: Theoretically, the two aldehydes of terephthalaldehyde (TPA) are equivalent, so the single or double Schiff base from TPA and D-glucosamine (Glc) may be formed at the same time. However, it is preferred to produce separately a single Schiff base (L_1) or double Schiff base (L_2) for different synthesis systems of anhydrous methanol or water−methanol. We calculated the $\Delta_r G$ of the formation of compounds L_1 and L_2 by density functional theory (DFT). In an anhydrous methanol system, the $\Delta_r G$ values of L_1 and L_2 are both below zero and L_2 is lower, suggesting the spontaneous formation of the two Schiff bases. Though adjusting the molar ratio of Glc to TPA, L_1 and L_2 both were separately formed in anhydrous methanol. However, in the water−methanol system, L_2 was absent, which is most likely due to higher $\Delta_r G$ (4.95 eV) and better water solubility. The results also exhibits that the positive charge of C in −CHO for TPA is smaller in a mixed solvent than that in methanol, which confirms that the nucleophilic reaction of the Schiff base is more difficult in a mixed solvent. Therefore, we could realize to control the synthesis of a pure single or double Schiff base from Glc and TPA by adjusting the molar ratio and solvent. The as-prepared two kinds of Schiff bases have strong optical properties, high bacteriostatic activity, and can be used as fluorescent probes for tumor cell imaging.

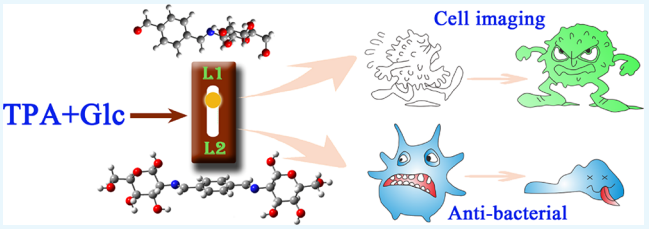

INTRODUCTION

Condensation of carbonyl compounds with primary amines was discovered in 1864 by Hugo Schiff.[1] Thus, this kind of compound is hereafter called the Schiff base. It refers to the reaction between a class of compounds containing aldehydes and the others with amino groups, which results in imine groups (—C═N—).[2−4] The Schiff base is not only used as a pigment, dye, catalyst, intermediate in organic synthesis, a supercapacitor, and so on[5−8] but also shows a wide range of biological activities, including anti-fungal, anti-bacterial, anti-malaria, anti-proliferation, anti-inflammatory, anti-virus, etc.[9−13]

As a natural amino monosaccharide, D-glucosamine (Glc) exists in a variety of organisms, and it has excellent biological activity.[14−19] It has a good killing effect on cancer cells but has little cytotoxicity to normal human cells.[20,21] Currently, Glc and its derivatives have attracted more attention due to their special nature of the molecular structure, one amino group, and four hydroxyls. In addition, the various products have been applied in many fields like biology, medicine, and so on.[22] The amino group can condense with aldehyde compounds to prepare the Schiff base. If sugar is introduced into the structure of the Schiff base, then it is expected that the drugs with less toxicity and better anticancer activity can be obtained. In addition, Glc contains rich hydroxyl groups, which can make the synthesized Schiff base with good water solubility. Therefore, the synthesis of the Schiff base with Glc as a lead compound has important significance in the field of biomedicine and other fields.[23]

At present, some scholars have reported the Schiff bases from Glc; however, few bis-Schiff bases were synthesized from Glc. In this work, we report a single Schiff base and a symmetric bis-Schiff base (marked as L_1 and L_2) both from Glc and terephthalaldehyde (TPA). According to previous works,[24,25] the synthesis process of the compounds is designed, as shown in Figure 1, and the two Schiff bases can be separated by adjusting the solvent and molar ratio. The two compounds are with good water solubility, optical properties, and bacteriostatic activity, which could be applied for biological imaging and anti-bacteria.

RESULTS AND DISCUSSION

Schiff bases L_1 and L_2 were synthesized in different synthesis methods. In the first method (M_1), Glc and TPA of different proportions were mixed in anhydrous methanol and reacted

Received: July 27, 2020
Accepted: September 7, 2020
Published: September 16, 2020

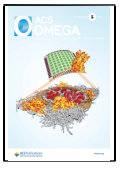

https://dx.doi.org/10.1021/acsomega.0c03591
ACS Omega 2020, 5, 24864−24870

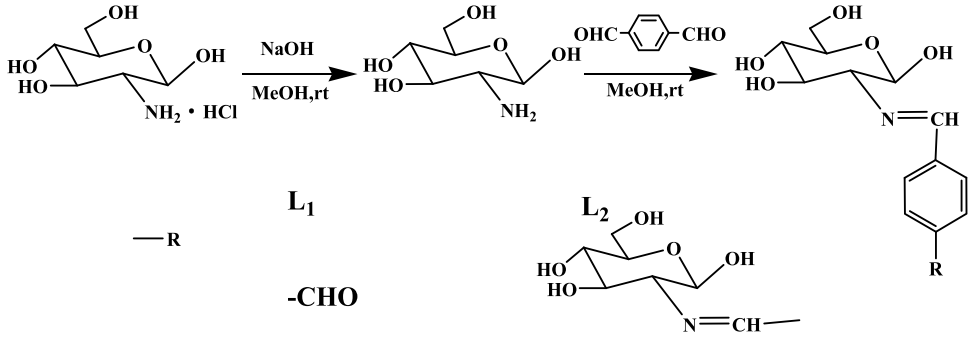

Figure 1. Synthesis of Schiff bases L_1 and L_2.

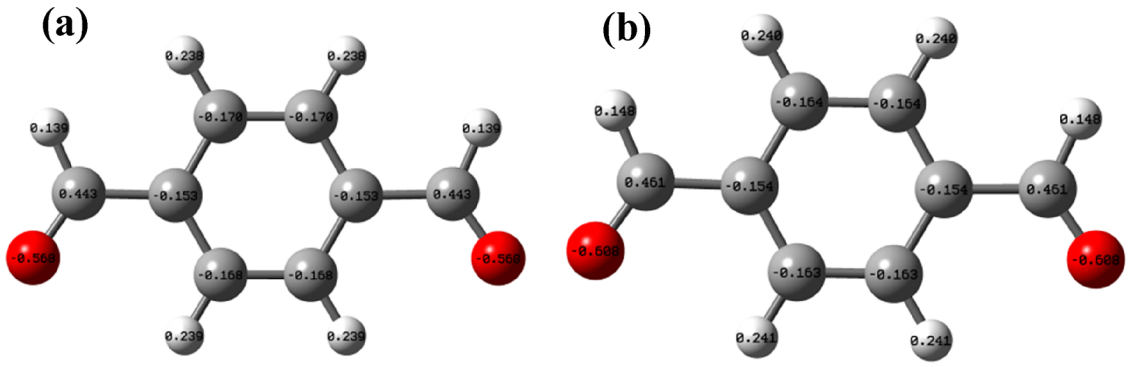

Figure 2. Atomic charges of TPA in (a) water−methanol and (b) methanol.

for 50 min at 35 °C and then stood overnight. The difference in the second method (M_2) was that it was a mixed solvent of water and methanol where TPA methanol solution was added into Glc aqueous solution and stirred at room temperature for 3 h. The two aldehydes of TPA are equivalent in theory, so the single or double Schiff base should be formed at the same time. However, the results show that, in the anhydrous methanol synthesis system, the product was changed from L_1 to L_2 when the molar ratio of Glc to TPA was from 1:1 to higher than 2:1. However, in water−methanol solution, only L_1 was formed even if the molar ratio was higher than 2:1.

As seen from Figure S2, ^{1}H NMR and ^{13}C NMR spectra of compounds L_1 and L_2 are without impurity peak, which proves that the two Schiff bases have high purity. Using compound L_1 as an example, characteristic peaks of —HC═N— appear in both ^{13}C NMR spectra at 161.79 ppm and ^{1}H NMR spectra at 8.32 ppm, indicating that the Schiff base was successfully synthesized. Furthermore, the characteristic peaks of −CHO at 193.40 ppm for ^{13}C NMR and 10.07 ppm for ^{1}H NMR also appear for L_1, which indicates that only one −CHO is replaced. For L_2, the peaks of −CHO in ^{1}H NMR and ^{13}C NMR spectra are absent.

To explore the synthesis mechanism, we calculated $\Delta_r G$ of compounds L_1 and L_2 synthesized by two methods, and the values of $\Delta_r G$ are as follows. Based on the optimized structures, the zero-point-corrected Gibbs free energies (G) at 298.15 K were calculated at the ωB97XD/6-311++g(d, p) level to obtain $\Delta_r G$ of the considered reactions. As ΔG shows, in an anhydrous methanol system, the $\Delta_r G$ values of L_1 and L_2 are both below zero, suggesting the spontaneous formation of the two Schiff bases in which L_2 is easier to generate. Nevertheless, with the water−methanol method, the value of $\Delta_r G$ is higher than that prepared with M_1. Furthermore, the $\Delta_r G_{2,2}$ value is up to 4.95, which indicates the difficult formation of L_2, and this phenomenon coincides with the experimental results. The results show that the water solubility of L_2 (20 mg/mL) with rich −OH is stronger than that of L_1 (16 mg/mL), although it is highly symmetrical. Furthermore, the positive charge of C in −CHO for TPA is smaller in the mixed solvent than that in methanol (Figure 2). The reason for varied charge distribution is that the salvation and dipole moment reduce in water−methanol, resulting in a decrease of charge separation. Because the formation of the Schiff base is a nucleophilic reaction, the low positive charge of C means that the synthesis reaction could be difficult. In the water−methanol system, the absence of L_2 is most likely due to lower positive charge of C atom in −CHO, good solubility, and higher formation energy in this system.

$$\text{Glc} + \text{TPA} \rightarrow \mathbf{L_1} + H_2O;\ M_1\text{: } \Delta_r G_{1,1} = -3.75;\ M_2 \text{: } \Delta_r G_{2,1} = 0.28$$

$$2\text{Glc} + \text{TPA} \rightarrow \mathbf{L_2} + 2H_2O;\ M_1\text{: } \Delta_r G_{1,2} = -5.05;\ M_2 \text{: } \Delta_r G_{2,2} = 4.95$$

where the units are in kcal/mol.

The highest occupied molecular orbital (HOMO) and lowest unoccupied molecular orbital (LUMO) are critical parameters to characterize the kinetic stability of the molecule, and the energy gap between HOMO and LUMO determines the molecular chemical reactivity and stability and explains the intermolecular electrical transport.[26] The orbital distributions and energies of HOMO and LUMO have been performed for the two compounds in different solvents at the ωB97XD/6-311++g(d, p) level. Orbital distributions and energies of HOMO and LUMO in different solvents are shown in Figure 3. It can be found that HOMO electrons are localized over the

https://dx.doi.org/10.1021/acsomega.0c03591
ACS Omega 2020, 5, 24864−24870

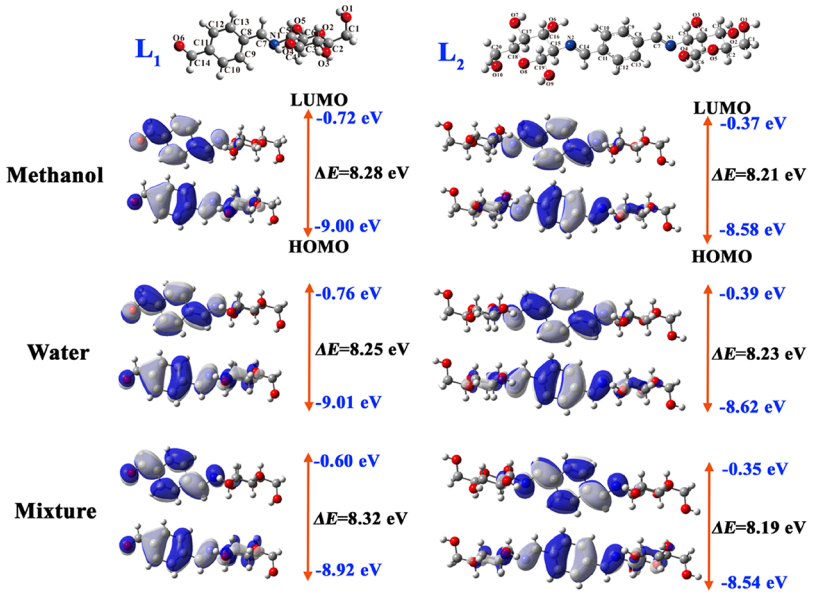

Figure 3. Optimized structures, molecular orbital, and energy level in different solvents for Schiff bases L_1 and L_2.

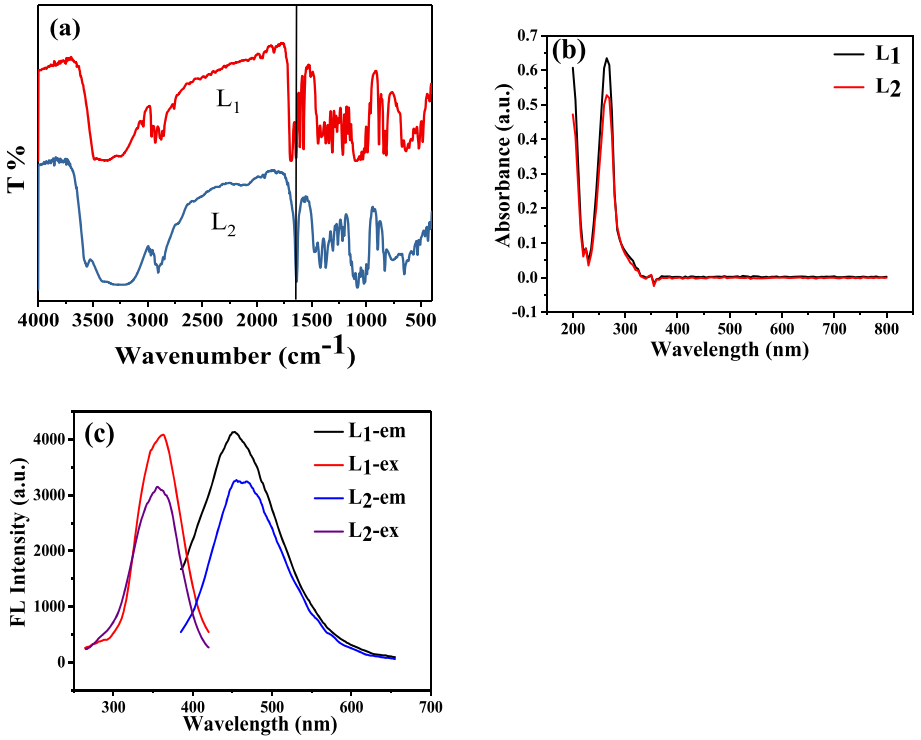

Figure 4. (a) FT-IR spectra, (b) UV−vis absorption spectra, and (c) fluorescence excitation and emission spectra of Schiff bases L_1 and L_2.

glucose, C═N, benzene, and aldehyde of compounds L_1 and L_2. Meanwhile, LUMO electrons have a centralized distribution in C═N, benzene, and aldehyde of compounds L_1 and L_2. The orbital energies of HOMO and LUMO for both L_1 and L_2 in a mixed solvent are higher than those in pure methanol or water. As seen in Figure 3, L_1 has a lower LUMO energy level and L_2 has a higher HOMO energy level. It indicates that L_1 is likely to behave as an electron acceptor, and L_2 presents as an electron donor. The energy gap between HOMO and LUMO for compound L_1 is the largest in the mixed solvent but that for L_2 is the smallest. However, the energy gaps for L_1 and L_2 in the three kinds of solvents are all larger than 8.0 eV, which means good stability of the two compounds.

The organic functional groups of the two compounds were analyzed by Fourier transform infrared (FT-IR) spectra. Figure 4a depicts the FT-IR spectra of compounds L_1 and L_2, and the data is shown in Table S1. The C═N stretching vibration, which is the most characteristic band of the Schiff base derivatives, occurs at 1640 cm^{-1}. The OH stretching bands of the Glc group of compound L_1 are observed in 3481 cm^{-1}, while the C−OH stretching bands are found at 1268, 1219, 1165, and 1151 cm^{-1}. The observed bands at 603, 573, and 549 cm^{-1} can be assigned to the pyranose skeleton, and the

https://dx.doi.org/10.1021/acsomega.0c03591
ACS Omega 2020, 5, 24864−24870

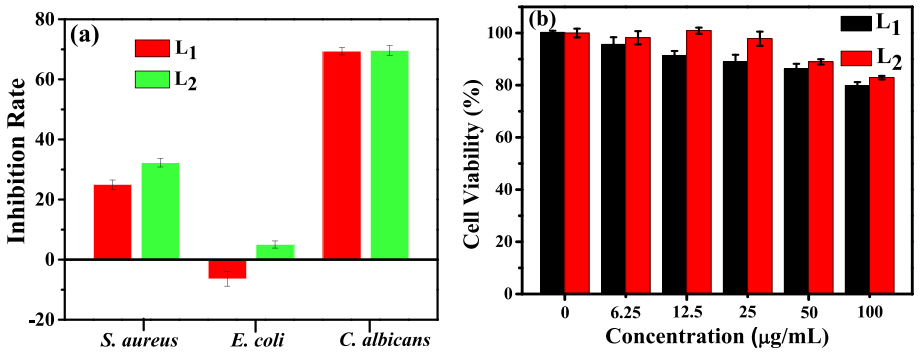

Figure 5. (a) Anti-bacterial activity against *S. aureus*, *E. coli*, and *C. albicans*. (b) Cytotoxicity on HepG2 cells for Schiff bases L_1 and L_2.

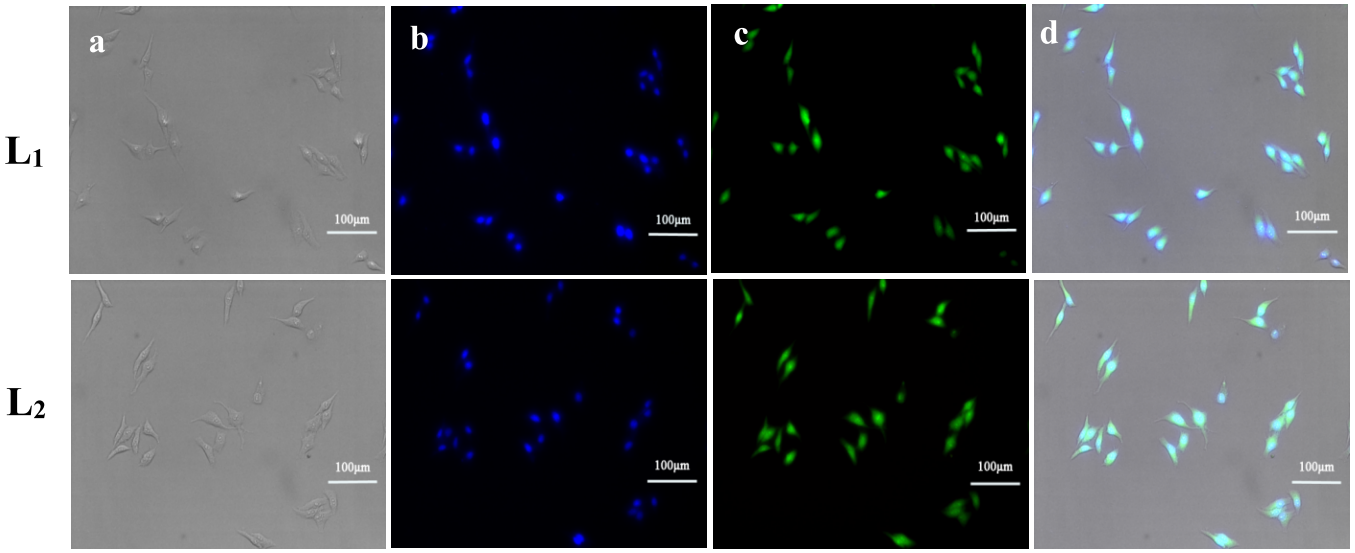

Figure 6. Inverted fluorescence imaging of HepG2 cells with 20× objectives. (a) Bright-field image of HepG2 cells, (b) HepG2 cells stained with DAPI, (c) HepG2 cells stained with the Schiff bases, and (d) the overlay image.

band at 1087 cm^{-1} belongs to pyran ether. The C═C bands of the aromatic nucleus are observed at 1572, 1439, and 1410 cm^{-1}. Characteristic absorption peaks of C═N, the sugar ring, and the aromatic nucleus appear in FT-IR spectra at the same time, which illustrates the formation of the Schiff base. What is more, the FT-IR spectra of compound L_1 show the characteristic absorption peaks of −CHO at 1689 cm^{-1} while those of compound L_2 disappear, which proves that the two −CHO groups are all replaced and also confirms the formation of compound L_2.

The UV−vis absorption spectra of the compounds (1 mg/mL) in ultrapure water were recorded within 200−800 nm at room temperature. From Figure 4b, we can see that the spectra of the two Schiff bases are similar. The strong absorption peak at 200 nm is caused by the $\pi-\pi^*$ transition of the C═N connected with the sugar ring. The absorption peak of aromatic aldehydes is generally about 250 nm,[25] while the Schiff bases have a stronger absorption due to the larger conjugated carbon π-system. The absorption peaks of compounds L_1 and L_2 can be attributed to $n-\pi^*$ at 266 nm.

The fluorescence excitation and emission spectra of Schiff bases (1 mg/mL) in ultrapure water were determined at room temperature (see Figure 4c). The excitation wavelength was 360 nm, and the emission wavelength was about 450 nm. Since the Schiff base molecules contain a π-electron conjugated system and an aromatic nucleus with a rigid plane structure, the synthesized molecules L_1 and L_2 have good fluorescence performance. The emission QY values of L_1 and L_2 are 5.65 and 15.28%, respectively. It can be seen from Figure 3c that the different substituents attached to the aromatic nucleus caused different fluorescence wavelengths. Even so, the fluorescence spectra are very similar due to similar structures.

To research the anti-bacterial activity of compounds L_1 and L_2, the OD600 of the bacteria after being treated with the two Schiff bases (0.08 mg/mL) for 24 h were recorded, including *Staphylococcus aureus*, *Escherichia coli*, and *Candida albicans*. As shown in Figure 5a, L_1 and L_2 at the low concentration have the best bacteriostatic effect on *C. albicans* with an inhibition rate of about 70% and the second one is *S. aureus*. L_2 has a certain inhibitory effect on *E. coli*, whereas L_1 has no inhibitory effect on *E. coli* at all. Nevertheless, as shown in Figure S1a, the inhibition rates of Glc (0.08 mg/mL) against *S. aureus*, *E. coli*, and *C. albicans* are 3.26, 12.04, and 2.58%, respectively, and those for TPA are 8.00, 15.66, and 2.79%, respectively. Overall, the two Schiff bases synthesized in this study have good bacteriostatic activity, which is competitive compared with other Schiff bases derived from D-glucosamine.[27] It can also be found that the bacteriostatic effect of L_2 is better than that of L_1. The previous study has established that the presence of imine or azomethine subunits in various compounds was critical to their biological activities.[28] Accordingly, the

https://dx.doi.org/10.1021/acsomega.0c03591
ACS Omega 2020, 5, 24864−24870

bacteriostatic activity of the double Schiff base (L_2) is better than that of the single Schiff base (L_1).

For the study of cytotoxicity for the two Schiff bases, the MTT test was carried out. In the test, the human hepatocellular carcinoma cells (HepG2 cells)[29] were dyed with 3-(4,5-dimethyl-2-thiazolyl)-2,5-diphenyl-2*H*-tetrazolium bromide (MTT) and treated with various concentrations of the two compounds for 24 h. Then, an absorbance at 490 nm was measured to calculate the cell survival rate. The larger the absorption at 490 nm after drug treatment, the smaller the cytotoxicity. Figure 5b displays the cytotoxicity of compounds L_1 and L_2 to HepG2 cells. The cell survival rate is more than 70% at even a concentration of 100 μg/mL. At the same contration, the cell survival rate of TPA is lower than 55% (Figure S1b). This demonstrates that both L_1 and L_2 have low cytotoxicity and good biocompatibility, which provided potential possibilities for bioimaging. Overall, because of the −CHO of L_1, the cytotoxicity of L_1 is higher than that of L_2.

The feasibility of fluorescence imaging with compounds L_1 and L_2 in HepG2 cells was studied (Figure 6). It exhibits that compounds L_1 and L_2 can be used as a fluorescent probe for tumor cell imaging. The bright-field images of HepG2 cells and HepG2 cells stained with 4′,6-diamidino-2-phenylindole (DAPI) are shown in Figure 5a and Figure 5b, respectively. After being incubated with compounds L_1 and L_2 for 1 h, the HepG2 cells show a clear and bright green fluorescence stimulated by a blue channel, and the image background is clean. It demonstrates that compounds L_1 and L_2 have excellent permeability of the cell membrane, which made it easy to dye HepG2 cells (Figure 5c). In addition, the overlay image in Figure 5d displays that the staining position of compounds L_1 and L_2 on cells overlaps with that of DAPI nuclear dyes, and the cytoplasmic part also shows the green fluorescence, which indicates that compounds L_1 and L_2 can enter both the cytoplasm and nucleus.

d

CONCLUSIONS

In this work, two new Schiff bases L_1 and L_2 were prepared, which have strong optical properties and high anti-bacterial activity. Therefore, the prepared Schiff bases can be used as fluorescent probes for tumor cell imaging. Comparing the two compounds, the advantages of water solubility, bacteriostatic activity, and cytotoxicity of L_2 are better than those of L_1. It is worth noting that we have realized the controllable synthesis of single and double Schiff bases by adjusting the molar ratio of Glc to TPA and explained the selection of the reaction mechanism.

EXPERIMENTAL SECTION

All chemicals were obtained from commercial suppliers and used without further purification. The ^{1}H and ^{13}C NMR spectra were recorded in DMSO-d_6 on a Bruker ascend 500 m spectrometer operating at 500 and 126 MHz. Mass spectrometry was collected by a Solan 70 FT-MS high-resolution mass spectrometer in DMSO with an electrospray ionization source (ESI). IR spectra were obtained using a Nicolet IS50 FT-IR spectrometer with KBr pellets in the range of 400−4000 cm^{-1}. The data of elemental analysis were measured by an Elemantar Vario EL cube organic element analyzer. UV−vis spectra were measured using a Shimadzu UV-2600 spectrophotometer. Fluorescence measurement was performed at room temperature on a Cary Eclipse fluorescence spectrometer in a 300 μL quartz cuvette. Cell imaging was performed on a DFC450C inverted fluorescence microscope (Leica, Germany).

Synthesis of Schiff Base. Glc hydrochloride (2.5 mmol), NaOH (2.5 mmol), and anhydrous methanol (5 mL) were added into a 50 mL beaker. The mixture was stirred and refluxed for 5 min, and then, NaCl was filtered out.

Terephthalaldehyde (TPA) (2.5 mmol) anhydrous methanol solution was slowly added to the filtrate and reacted for 50 min by stirring at 35 °C. The white precipitate was formed for one night. Finally, the solid was filtered and washed several times with cold anhydrous methanol. This is the first system to prepare the Schiff base, marking as M_1. Compound L_1 was obtained by air drying (yield 70.98%). M.wt.: 295.286; MS (ESI) ([M + Na]$^+$) = 318.095 (Figure S3). ^{1}H NMR (500 MHz, DMSO-d_6), δ ppm, 2.91 (t, 1H, CH_2), 3.18−3.49 (m, 4H, GlcH), 3.70−3.78 (m, 1H, CH_2), 4.62 (t, 1H, OH), 4.78 (t, 1H, OH), 4.98 (d, 1H, CH-N), 5.04 (d, 1H, OH), 6.67 (d, 1H, OH), 7.99 (s, 4H, ArH), 8.32 (s, 1H, —CH═N—), 10.07 (s, 1H, −CHO) (Figure S2). ^{13}C NMR (126 MHz, DMSO-d_6), δ ppm, 95.87−61.68 (6C, GlcC), 141.61−129.04 (4C, ArC), 161.79 (1C, —C═N—), 193.40 (1C, −CHO) (Figure S2).[25]

The synthetic method of compound L_2 was similar to that of L_1 where the amount of TPA was changed to 1 mmol, and the other steps were the same (yield 51.80%). M.wt.: 456.444; MS (ESI) ([M + Na]$^+$) = 479.164 (Figure S3). ^{1}H NMR (500 MHz, DMSO-d_6), δ ppm, 2.93−2.84 (m, 1H, CH_2), 3.17−3.54 (m, 4H, GlcH), 3.70−3.78 (ddd, 1H, CH_2), 4.59 (t, 1H, OH), 4.75 (t, 1H, OH), 4.92 (d, 2H, CH-N), 4.98 (d, 1H, OH), 6.62 (d, 1H, OH), 7.83 (s, 2H, ArH), 8.25 (s, 1H, —CH═N—) (Figure S2). ^{13}C NMR (126 MHz, DMSO-d_6), δ ppm, 95.94−61.69 (6C, GlcC), 138.31−128.68 (4C, ArC), 162.13 (1C, —C═N—) (Figure S2) .

For the second method (marked as M_2), due to the different solubility of Glc and TPA, the water−methanol method was used to synthesize the Schiff base. Glc hydrochloride (2.5 mmol), $NaHCO_3$ (2.5 mmol), and ultrapure water (5 mL) were added to a 50 mL beaker. After complete dissolution, 5 mL of 2.5 mmol of TPA anhydrous methanol solution was added and the mixture was stirred at room temperature for 3 h. Compound L_1 was obtained overnight from the reaction solution. Surprisingly, no compound L_2 was formed even if the amount of TPA was changed to 1 mmol (yield 73.95%). The elemental analysis of compounds L_1 and L_2 is shown in Table 1.

Table 1. Elemental Analysis of Compounds L_1 and L_2

compound	measured value	theoretical value
L_1	C56.40, H5.80, O33.39, N4.47	C56.95, H5.75, O32.54, N4.75
L_2	C49.04, H6.68, O38.67, N5.61	C52.62, H6.18, O35.05, N6.14

Computational Procedures. All the density functional theoretical (DFT) calculations in this work were carried out by using the ωB97XD density functional in conjunction with the 6-311++G(d, p) split valence basis set in the GAUSSIAN 16 software package.[30] The analyses of vibration frequencies have been also implemented at the same theoretical level to make sure that all the optimized structures are true minima without any imaginary frequencies on their potential energy surfaces. Based on the optimized structures, the zero-point-corrected

https://dx.doi.org/10.1021/acsomega.0c03591
ACS Omega 2020, 5, 24864−24870

Gibbs free energies (G) at 298.15 K were calculated at the ωB97XD/6-311++g(d, p) level to obtain $\Delta_r G$ of the considered reactions. The solvation model based on density (SMD)[31] was used to take the effect of the solvent into account in all the calculations. Dimensional plots of molecular configurations and orbitals were generated with the GaussView program.[32]

Anti-Bacterial Activity. The anti-bacterial activity of the drugs (compounds $\mathbf{L_1}$ and $\mathbf{L_2}$) was studied by the 96-well plate titration method. The bacteria were plated in a Luria−Bertani (LB) medium composed of tryptone, yeast extract, and sodium chloride. The specific process was as follows: *S. aureus*, *E. coli*, and *C. albicans* were resuscitated by adding 5 mL of the LB medium to the freeze-dried bacterial powders overnight. After that, amplification was cultured by adding 5 mL of the LB medium to 1 mL of the resuscitated bacterial solutions. The experiment was carried out when the value of OD 600 nm reached 0.6 (logarithmic growth period). We prepared 0.08 mg/mL of the drugs with ultrapure water. The *S. aureus*, *E. coli*, and *C. albicans* solution were evenly planted into a 96-well plate with 100 μL per hole, and then, the drug solutions were added into the plate with 100 μL per hole. The value of OD 600 nm was measured after incubating at 37 °C for 24 h.

Cytotoxicity Study. The cytotoxicity of compounds $\mathbf{L_1}$ and $\mathbf{L_2}$ to HepG2 cells was studied following a reported MTT test. 3-(4,5-Dimethyl-2-thiazolyl)-2,5-diphenyl-2*H*-tetrazolium bromide (MTT)[33] is a yellow dye, which can specifically recognize living cells. Briefly, (i) HepG2 cells in the logarithmic phase were seeded into a 96-well plate at 10,000 cells per well and grown in an incubator (37 °C, 5% CO_2) for 24 h. (ii) These cells were incubated with 100 μL of compounds $\mathbf{L_1}$ or $\mathbf{L_2}$ (0, 6.25, 12.5, 25, 50, and 100 μg/mL) for 24 h. (iii) MTT solution (100 μL, 1 .0 mg/mL) was added into each well and then coincubated for 4 h. (iv) The supernatant was removed, and 150 μL of DMSO was added. The absorbance at 490 nm was measured by a microplate reader after shaking for 10 min. (v) The cell survival rate was acquired by $A/A_0 \times 100\%$ (A and A_0 represent the absorbance of the $\mathbf{L_1}$ or $\mathbf{L_2}$ treat group and control group, respectively).

In Vitro Cell Imaging. Human cancer cells were seeded into a Petri dish at a density of 10×10^4 cells per well and cultured in a Roswell Park Memorial Institute (RPMI) medium supplemented with 10% fetal bovine serum (FBS) and 1% PS in an incubator (37 °C, 5% CO_2) for 24 h. Then, the medium was removed and the adherent cells were washed with phophate-buffered saline (PBS) three times. Subsequently, 1 mL of the incomplete medium containing compounds $\mathbf{L_1}$ or $\mathbf{L_2}$ (39.22 μg/mL) was added to the wells. After incubation for 1 h, the medium was cleaned with PBS three times and dyed with 4′,6-diamidino-2-phenylindole (DAPI) (1 μg/mL) PBS solution for 10 min. DAPI can emit a blue fluorescence to sign the cell nucleus.[34] Then, it was cleaned with PBS twice, and 1 mL of 2.5% GD was used to fixed cells for 10 min. Before imaging, the solution was removed, and then, the cells were washed with PBS three times. The bright-field and fluorescent images of cells were obtained on an inverted fluorescence microscope.

■ ASSOCIATED CONTENT

Supporting Information

The Supporting Information is available free of charge at https://pubs.acs.org/doi/10.1021/acsomega.0c03591.

Mass spectrometry, the data of FT-IR spectra, ^{1}H NMR and ^{13}C NMR for the prepared compounds, and more details for the computational procedures (PDF)

■ AUTHOR INFORMATION

Corresponding Authors

Jie Kang − *School of Pharmacy, Fujian Medical University, Fuzhou 350122, P R China*; Email: davidkj660825@163.com

Zhizhong Han − *School of Pharmacy, Fujian Medical University, Fuzhou 350122, P R China; Fujian Key Laboratory of Drug Target Discovery and Structural and Functional Research, Fuzhou 350122, P R China*; orcid.org/0000-0001-7888-5601; Email: zzhan@fjmu.edu.cn

Authors

Qinghua Weng − *School of Pharmacy, Fujian Medical University, Fuzhou 350122, P R China; Fujian Key Laboratory of Drug Target Discovery and Structural and Functional Research, Fuzhou 350122, P R China*

Jinquan Yi − *School of Pharmacy, Fujian Medical University, Fuzhou 350122, P R China; Fujian Key Laboratory of Drug Target Discovery and Structural and Functional Research, Fuzhou 350122, P R China*

Xiaoping Chen − *School of Pharmacy, Fujian Medical University, Fuzhou 350122, P R China; Fujian Key Laboratory of Drug Target Discovery and Structural and Functional Research, Fuzhou 350122, P R China*

Dengwang Luo − *School of Pharmacy, Fujian Medical University, Fuzhou 350122, P R China; Fujian Key Laboratory of Drug Target Discovery and Structural and Functional Research, Fuzhou 350122, P R China*

Yaduan Wang − *School of Pharmacy, Fujian Medical University, Fuzhou 350122, P R China*

Weiming Sun − *School of Pharmacy, Fujian Medical University, Fuzhou 350122, P R China; Fujian Key Laboratory of Drug Target Discovery and Structural and Functional Research, Fuzhou 350122, P R China*; orcid.org/0000-0002-9882-0511

Complete contact information is available at: https://pubs.acs.org/10.1021/acsomega.0c03591

Notes

The authors declare no competing financial interest.

■ ACKNOWLEDGMENTS

The authors gratefully acknowledge the financial support from the National Natural Science Foundation of China (51602053), Joint Funds for the Innovation of Science and Technology, Fujian Province (2017Y9122), the Fujian Natural Science Foundation (2019 J01300), the Program for New Century Excellent Talents in Fujian Province University (2018B031), and the Fujian Province Special Funds for Science and Technology Special Commissioners.

■ REFERENCES

(1) Borisova, N. E.; Reshetova, M. D.; Ustynyuk, Y. A. Metal-Free Methods in The Synthesis of Macrocyclic Schiff bases. *Chem. Rev.* **2007**, *107*, 46−79.

(2) Jia, Y.; Li, J. Molecular assembly of Schiff base interactions: construction and application. *Chem. Rev.* **2015**, *115*, 1597−1621.

(3) Arabahmadi, R.; Amani, S. A new fluoride ion colorimetric sensor based on azo-azomethine receptors. *Supramol. Chem.* **2014**, *26*, 321−328.
(4) da Silva, C. M.; da Silva, D. L.; Modolo, L. V.; Alves, R. B.; de Resende, M. A.; Martins, C. V. B.; de Fátima, Â. Schiff bases: a short review of their antimicrobial activities. *J. Adv. Res.* **2011**, *2*, 1−8.
(5) Nejati, K.; Rezvani, Z.; Massoumi, B. Syntheses and investigation of thermal properties of copper complexes with azo-containing Schiff-base dyes. *Dyes Pigm.* **2007**, *75*, 653−657.
(6) Gupta, K. C.; Sutar, A. K. Catalytic activities of Schiff base transition metal complexes. *Coordin. Chem. Rev.* **2008**, *252*, 1420−1450.
(7) Xue, D.; Zhu, D.; Liu, M.; Duan, H.; Li, L.; Chai, X.; Wang, Z.; Lv, Y.; Xiong, W.; Gan, L. Schiff-base/resin copolymer under hypersaline condition to high-level N-doped porous carbon nanosheets for supercapacitors. *ACS Appl. Nano Mater.* **2018**, *1*, 4998−5007.
(8) Vikneshvaran, S.; Velmathi, S. Impact of halide-substituted chiral Schiff bases on corrosion behaviour of carbon steel in acidic environment. *J. Nanosci. Nanotechno.* **2019**, *19*, 4458−4464.
(9) Arif, R.; A, m.; Ahmed, S.; Ahmed, S.; Abid, M.; Rahisuddin. Synthesis, in vitro biological evaluation and in silico studies of some new heterocyclic Schiff bases. *Biol. Chem. Chem. Select.* **2018**, *3*, 13517−13525.
(10) Garoufis, A.; Hadjikakou, S. K.; Hadjiliadis, N. Palladium coordination compounds as anti-viral, anti-fungal, anti-microbial and anti-tumor agents. *Coordin. Chem. Rev.* **2009**, *253*, 1384−1397.
(11) Przybylski, P.; Huczynski, A.; Pyta, K.; Brzezinski, B.; Bartl, F. Biological properties of Schiff bases and azo derivatives of phenols. *Curr. Org. Chem.* **2009**, *13*, 124−148.
(12) Ko, H.-H.; Tsao, L.-T.; Yu, K.-L.; Liu, C.-T.; Wang, J.-P.; Lin, C.-N. Structure-activity relationship studies on chalcone derivatives: the potent inhibition of chemical mediators release. *Bioorgan. Med. Chem.* **2003**, *11*, 105−111.
(13) Domínguez, J. N.; Charris, J. E.; Lobo, G.; de Domínguez, N. G.; Moreno, M. M.; Riggione, F.; Sanchez, E.; Olson, J.; Rosenthal, P. J. Synthesis of quinolinyl chalcones and evaluation of their antimalarial activity. *Eur. J. Med. Chem.* **2001**, *36*, 555−560.
(14) Al-Hamidi, H.; Edwards, A. A.; Douroumis, D.; asare-Addo, K.; Nayebi, A. M.; Reyhani-Rad, S.; Mahmoudi, J.; Nokhodchi, A. Effect of glucosamine HCl on dissolution and solid state behaviours of piroxicam upon milling. *Colloids Surf., B* **2013**, *103*, 189−199.
(15) Guillemineau, M.; Auzanneau, F.-I. Challenging deprotection steps during the synthesis of tetra-and pentasaccharide fragments of the Le^aLe^x tumor-associated hexasaccharide antigen. *J. Org. Chem.* **2012**, *77*, 8864−8878.
(16) García-Álvarez, I.; Groult, H.; Casas, J.; Barreda-Manso, M. A.; Yanguas-Casás, N.; Nieto-Sampedro, M.; Romero-Ramírez, L.; Fernández-Mayoralas, A. Synthesis of antimitotic thioglycosides: in vitro and in vivo evaluation of their anticancer activity. *J. Med. Chem.* **2011**, *54*, 6949−6955.
(17) Shivatare, S. S.; Chang, S.-H.; Tsai, T.-I.; Ren, C.-T.; Chuang, H.-Y.; Hsu, L.; Lin, C.-W.; Li, S.-T.; Wu, C.-Y.; Wong, C.-H. Efficient convergent synthesis of bi-, tri-, and tetra-antennary complex type N-glycans and their HIV-1 antigenicity. *J. Am. Chem. Soc.* **2013**, *135*, 15382−15391.
(18) Walczak, M. A.; Danishefsky, S. J. Solving the convergence problem in the synthesis of triantennary N-glycan relevant to prostate-specific membrane antigen (PSMA). *J. Am. Chem. Soc.* **2012**, *134*, 16430−16433.
(19) Layek, B.; Singh, J. Cell penetrating peptide conjugated polymeric micelles as a high performance versatile nonviral gene carrier. *Biomacromolecules* **2013**, *14*, 4071−4081.
(20) Kobayashi, S.; Fukuda, T.; Yukimasa, H.; Fujino, M.; Ichiro, A.; Yuichi, Y. Synthesis, and the adjuvant and tumor-suppressive activities of quinonyl muramyl dipeptides. *B. Chem. Soc. Jpn.* **1984**, *57*, 3182−3196.
(21) Muzzarelli, R. A. A. Chitin and its derivatives: new trends of applied research. *Carbohyd. Polym.* **1983**, *3*, 53−75.
(22) Bruyere, O.; Pavelka, K.; Rovati, L. C.; Deroisy, R.; Olejarova, M.; Gatterova, J.; Giacovelli, G.; Reginster, J. Y. Glucosamine sulfate reduces osteoarthritis progression in postmenopausal women with knee osteoarthritis: evidence from two 3-year studies. *Menopause.* **2004**, *11*, 138−143.
(23) Costamagna, J.; Lillo, L. E.; Matsuhiro, B.; Noseda, M. D.; Villagrán, M. Ni (II) complexes with Schiff bases derived from amino sugars. *Carbohydr. Res.* **2003**, *338*, 1535−1542.
(24) Mitsunobu, O.; Yamada, M.; Mukaiyama, T. Preparation of esters of phosphoric acid by reaction of trivalent phosphorus compounds with diethyl azodicarboxylate in presence of alcohols. *B. Chem. Soc. Jpn.* **1967**, *40*, 935−939.
(25) Li, J. Y.; Liu, P. Synthesis of novel D-glucosamine Schiff bases. *Chinese J. Synthetic Chem.* **2006**, *14*, 523−525.
(26) Tadesse, S.; Alpaslan, Y. B.; Yildiz, M.; Ünver, H.; Aslan, K. Synthesis, characterization and applications of (E)-3-((5-bromo-2-hydroxy-3-methoxycy- clohexa-1,3-dienyl)methyleneamino)-6-(hydroxymethyl)-tetrahydro-2H-pyran-2,4,5- triol. *Nano Biomed. Eng.* **2016**, *8*, 72−81.
(27) Kumari, B.; Chauhan, K.; Trivedi, J.; Jaiswal, V.; Kanwar, S. S.; Pokharel, Y. R. Benzothiazole-based-bioconjugates with improved antimicrobial, anticancer and antioxidant potential. *ChemistrySelect* **2018**, *3*, 11326−11332.
(28) Xia, L.; Xia, Y.-F.; Huang, L.-R.; Xiao, X.; Lou, H.-Y.; Liu, T.-J.; Pan, W.-D.; Luo, H. Benzaldehyde Schiff bases regulation to the metabolism, hemolysis, and virulence genes expression in vitro and their structure-microbicidal activity relationship. *Eur. J. Med. Chem.* **2015**, *97*, 83−93.
(29) Dostál, Z.; Kosina, P.; Mlejnek, P.; Kikalová, K.; Modrianská, M. Mifepristone potentiates etoposide toxicity in Hep G2 cells by modulating drug transport. *Toxicol. In Vitro* **2019**, *54*, 33−40.
(30) Frisch, M. J.; Trucks, G. W.; Schlegel, H. B. *Gaussian 16,* Revision A.03; Gaussian, Inc.: Wallingford CT, USA, 2016.
(31) Marenich, A. V.; Cramer, C. J.; Truhlar, D. G. Universal solvation model based on solute electron density and on a continuum model of the solvent defined by the bulk dielectric constant and atomic surface tensions. *J. Phys. Chem. B* **2009**, *113*, 6378−6396.
(32) Dennington, R.; Keith, T.; Millam, J. *Gauss View, Version 5*; Semichem Inc.: Shawnee Mission, KS, 2009.
(33) Maehara, Y.; Kusumoto, T.; Kusumoto, H.; Anai, H.; Sugimachi, K. Sodium Succinate Enhances the Colorimetric Reaction of the in vitro Chemosensitivity Test: MTT Assay. *Oncology* **1988**, *45*, 434−436.
(34) Jia, T.; Xu, J.; Dong, S.; He, F.; Zhong, C.; Yang, G.; Bi, H.; Xu, M.; Hu, Y.; Yang, D.; Yang, P.; Lin, J. Mesoporous cerium oxide-coated upconversion nanoparticles for tumor-responsive chemo-photodynamic therapy and bioimaging. *Chem. Sci.* **2019**, *10*, 8618−8633.

https://dx.doi.org/10.1021/acsomega.0c03591
ACS Omega 2020, 5, 24864−24870